Available online at www.sciencedirect.com
ScienceDirect
Trans. Nonferrous Met. Soc. China 31(2021) 3905−3917
Transactions of Nonferrous Metals Society of China
www.tnmsc.cn

Thermodynamic analysis and process optimization of zinc and lead recovery from copper smelting slag with chlorination roasting

Bei-kai ZHANG[1], Xue-yi GUO[1,2,3], Qin-meng WANG[1,2,3], Qing-hua TIAN[1,2,3]

1. School of Metallurgy and Environment, Central South University, Changsha 410083, China;
2. National & Regional Joint Engineering Research Center of Nonferrous Metal Resources Recycling, Changsha 410083, China;
3. Hunan Key Laboratory of Nonferrous Metal Resources Recycling, Changsha 410083, China

Received 21 January 2021; accepted 10 August 2021

Abstract: An efficient chlorination roasting process for recovering zinc (Zn) and lead (Pb) from copper smelting slag was proposed. Thermodynamic models were established, illustrating that Zn and Pb in copper smelting slag can be efficiently recycled during the chlorination roasting process. By decreasing the partial pressure of the gaseous products, chlorination was promoted. The Box−Behnken design was applied to assessing the interactive effects of the process variables and optimizing the chlorination roasting process. $CaCl_2$ dosage and roasting temperature and time were used as variables, and metal recovery efficiencies were used as responses. When the roasting temperature was 1172 °C with a $CaCl_2$ addition amount of 30 wt.% and a roasting time of 100 min, the predicted optimal recovery efficiencies of Zn and Pb were 87.85% and 99.26%, respectively, and the results were validated by experiments under the same conditions. The residual Zn- and Pb-containing phases in the roasting slags were $ZnFe_2O_4$, Zn_2SiO_4, and PbS.

Key words: chlorination roasting; copper smelting slags; thermodynamic models; optimization; Zn and Pb recovery; Box−Behnken design

1 Introduction

As critical nonferrous metals, zinc (Zn) and lead (Pb) are widely used in machinery manufacturing, battery production, and galvanization [1]. In China, most smelters currently produce Zn and Pb with Pb−Zn symbiotic ore as the raw material by direct reduction and fuming processes [2]. After years of mining, the gradual depletion of high-grade Pb−Zn ore has forced smelters to recycle metallurgical secondary resources [3]. Moreover, the energy consumption of extracting metals from secondary resources is lower than that of extracting metals from primary resources [4].

Currently, the research in this field is focused on the comprehensive utilization of metallurgical slag [5,6]. HU et al [7] developed an integrated process for the recovery of Zn from Zn hydrometallurgy residue by roasting and water leaching in sequence. The results indicated that, under optimal conditions, the Zn recovery efficiency reached 90.9% and the leaching liquor could be directly returned to the Zn smelting. XIN et al [8] studied the recovery of Zn, Pb, and Sb from antimony smelting slag using a fuming furnace. The results showed that Zn, Pb, and Sb in antimony smelting slag could be recovered by the fuming furnace process, with metal recoveries of 88%, 95%, and 60%, respectively. PENG et al [9] presented a beneficiation−metallurgy combination process to

Corresponding author: Qin-meng WANG, Tel: +86-731-88876255, E-mail: qmwang@csu.edu.cn
DOI: 10.1016/S1003-6326(21)65773-4

recover Zn and Fe and enrich In and Ag from high-iron-bearing Zn calcine. The results demonstrated that 90% of Zn was extracted, and 83% of Fe was recovered during the process. Approximately 86% of In entered the iron concentration, whereas Ag mainly entered the tailings, with a recovery efficiency of 76%.

Copper smelting slag contains 1%−4% Zn and 0.2%−0.6% Pb [10]. However, it is difficult to recover Zn and Pb from copper smelting slag by traditional metallurgical processes because the slag has a stable structure and complicated multi-component system [11,12]. Chlorination roasting is a mature metallurgical method that can effectively separate and recover valuable metals from the smelting slag [13]. A pyrometallurgical process allows certain raw material components to react with the chlorinating agent to generate volatile chlorides at temperatures lower than their melting points [14]. Chlorinating agents generally include solid chlorinating agents ($CaCl_2$, NaCl, $MgCl_2$, NH_4Cl, etc.) and gaseous chlorinating agents (Cl_2, HCl, etc.) [15]. Although the gaseous chlorinating agent has a better chlorination effect, it is more likely to corrode the production pipeline [16]. Therefore, a solid chlorinating agent is preferable for use in chlorination roasting. Considerable research efforts have been devoted to the recovery of valuable metals from metallurgical slag by chlorination roasting. WANG et al [17] presented a novel process based on one-step chlorination roasting to simultaneously extract gold and Zn from refractory carbonaceous gold ore using NaCl as a chlorination agent. The results showed that the recovery efficiencies of gold and Zn were 92% and 92.56%, respectively, under optimal conditions. QIN et al [18] investigated the effect of chlorination roasting with pyrite on gold and silver recovery efficiencies from gold tailings. The results demonstrated that the addition of pyrite during the chlorination process promoted the recovery of gold and silver from gold tailings, and 98.56% of gold and 87.92% of silver were recovered under optimal conditions. Compared with other solid chlorinating agents, $CaCl_2$ is an ideal chlorinating agent because of its excellent removal performance on heavy metals at low cost [19]. During chlorination roasting, Ca from $CaCl_2$ is transformed into CaO, and the roasting slag can be further processed to prepare cement [20]. Consequently, $CaCl_2$ was used as the chlorinating agent in the present study.

Herein, an optimized chlorination roasting method was presented to recover Zn and Pb simultaneously from copper smelting slag, and the roasting mechanism was analyzed in detail. The Box−Behnken design is an efficient approach for fitting second-order polynomials to response surfaces and uses relatively small numbers of observations to estimate the parameters [21]. In the present study, the chlorination roasting process was modeled using the Box−Behnken design to obtain optimum conditions for recovering Zn and Pb and investigate the interaction among the critical process parameters such as $CaCl_2$ dosage and roasting temperature and time.

2 Experimental

2.1 Materials

The raw material used in the present study was copper smelting slag obtained from a copper smelter in Shandong Province, China, after dilution using a flotation method. The elemental content of the copper smelting slag was analyzed using an inductively coupled plasma emission spectrometer (ICP-OES), and the results are given in Table 1. The Zn and Pb contents were 2.80 and 0.45 wt.%, respectively. The phase composition of the copper smelting slag was determined using X-ray diffraction (XRD). The XRD pattern in Fig. 1(a) indicates that fayalite (Fe_2SiO_4), magnetite (Fe_3O_4), and zinc ferrite ($ZnFe_2O_4$) were the significant minerals present in the copper smelting slag. Because of the complex composition and structure of copper slags, the minor minerals are encapsulated in the significant minerals; therefore, they cannot be accurately characterized by XRD [22]. Chemical phase analysis is based on the difference in the solubility and dissolution rate of various minerals in chemical solvents, by using a selective dissolution method to accurately identify the mineral composition of raw materials [23]. Zn and Pb occurrences in the different phases of the copper smelting slag are shown in Tables 2 and 3, respectively. The Zn in the copper smelting slag was mainly Zn_2SiO_4, $ZnFe_2O_4$, ZnO, and ZnS, whereas only 0.36% of Zn was present as $ZnSO_4$. The Pb in the copper smelting slag was mainly PbS, $PbSiO_3$, $PbSO_4$, and PbO, whereas only 2.08% of Pb was present as metallic Pb. From the energy

Table 1 Chemical composition of copper smelting slag (wt.%)

Zn	Pb	Cu	Fe	O
2.80	0.45	0.55	41.23	36.10
Si	Ca	Na	K	S
11.75	1.76	1.36	0.58	0.41

Table 2 Occurrence of Zn in different phases of copper smelting slag

Phase	Content/(kg·t^{-1})	Distribution/%
Zn_2SiO_4	13.1	46.74
$ZnFe_2O_4$	9.75	34.79
ZnO	3.15	11.23
ZnS	1.93	6.88
$ZnSO_4$	0.1	0.36
Total	28.03	100

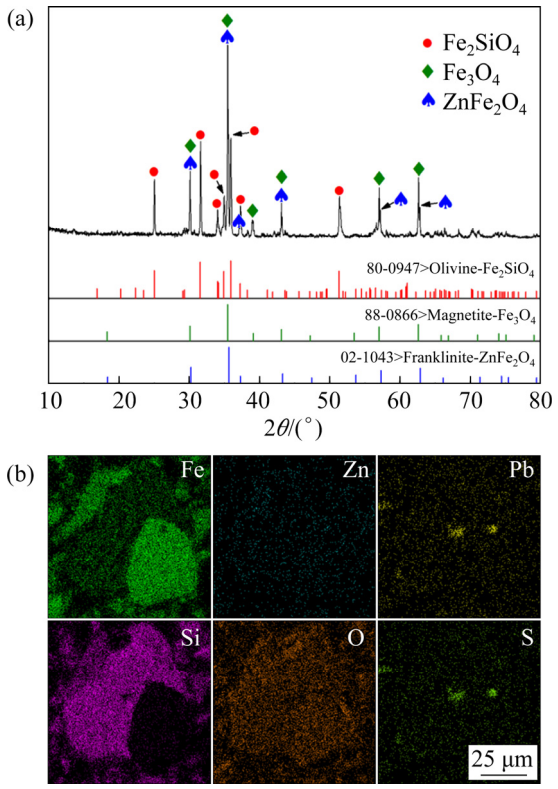

Fig. 1 XRD pattern (a) and EDS mappings (b) of copper smelting slag

dispersive spectroscopy (EDS) mapping of the copper smelting slag shown in Fig. 1(b), the Zn in the slag was encapsulated in fayalite and iron oxides, and the Pb in the slag was mainly combined with S, which was consistent with the aforementioned analysis results.

Table 3 Occurrence of Pb in different phases of copper smelting slag

Phase	Content/(kg·t^{-1})	Distribution/%
PbS	1.78	39.58
$PbSiO_3$	1.41	31.25
$PbSO_4$	0.66	14.59
PbO	0.56	12.5
Pb	0.094	2.08
Total	4.5	100

2.2 Experimental design

The Box−Behnken design is a response surface methodology suitable for experiments with limited factors [24]. In the present study, the Box−Behnken design was employed to evaluate the influence of the $CaCl_2$ dosage and the roasting temperature and time on the metal recovery efficiency. Thus, the optimum operating conditions for recycling were determined. The $CaCl_2$ dosage and roasting temperature and time are critical parameters during the chlorination roasting process. Specifically, without sufficient chlorinating agents during the roasting process, the Zn and Pb encapsulated in significant minerals cannot be converted into chlorides. The thermodynamic calculations show that the chlorination reaction of Zn and Pb was restricted at low temperatures. It is necessary to provide sufficient roasting time to ensure an adequate reaction. The chlorination reaction process might be adversely affected by excessive experimental parameters. For instance, the materials can be melted under an excessively high roasting temperature, resulting in the solidification of heavy metals, which can be converted into oxides during the long chlorination roasting time, and the cost can be increased using excessive chlorinating agent [25,26].

Three levels for each parameter were chosen: $CaCl_2$ dosage (10, 20, and 30 wt.%), roasting temperature (700, 950, and 1200 °C), and roasting time (30, 60, and 90 min). The Zn and Pb recovery efficiencies were chosen as the response variables. The variables and their levels are presented in Table 4. The polynomial equation modeling of the response variable as a function of the operating parameters studied was expressed as follows [27]:

$$Y = \beta_0 + \sum_{i=1}^{n} \beta_i x_i + \sum_{i=1}^{n} \beta_{ii} x_i^2 + \sum_{i<j}^{n} \beta_{ij} x_i x_j + k \quad (1)$$

where Y is the predicted response (Zn and Pb recovery efficiencies), n is the number of the patterns, i and j are the index numbers for the patterns, β_0 is the constant coefficient, β_i is the linear coefficient, β_{ii} is the quadratic coefficient, β_{ij} is the interaction coefficient, x_i and x_j are the coded independent variables, and k is the random error.

Table 4 Independent variables and their levels used for response surface methodology

Parameter	Code	Level		
		−1	0	1
$w(CaCl_2)$/wt.%	x_1	10	20	30
Temperature/°C	x_2	700	950	1200
Time/min	x_3	30	60	90

2.3 Experimental set-up and procedures

All Box−Behnken design experiments were conducted in a high-temperature tube furnace. A 20 g sample of dried copper smelting slag was ground and mixed with different $CaCl_2$ dosages, loaded in a corundum porcelain boat, and placed in a tube furnace. The temperature of the furnace was heated to a preset temperature at a heating rate of 10 °C/min, and air was then introduced at a flow rate of 100 mL/min. The raw materials were entirely roasted by holding them for a specified duration. Eventually, the roasting slags were recovered and ground into powder. The air was cut off when the furnace was cooled to room temperature (25−30 °C). During the experiment, the volatilized flue gas was gathered through a gas scrubber containing 200 mL of 10% NaOH at the tube furnace outlet. The Zn and Pb recovery efficiencies are presented in Eq. (2):

$$R=\frac{w_g \cdot m_g - w_s \cdot m_s}{w_g \cdot m_g} \tag{2}$$

where R is the recovery efficiency (%), w_g is the mass fraction of an element in the copper smelting slag, m_g is the mass of the copper smelting slag in the porcelain boat, w_s is the mass fraction of an element in the roasting slag, and m_s is the mass of the roasting slag.

2.4 Characterization and analyses

The experimental design and analyses were performed using Design-Expert 12. A high-temperature smelting quartz tube furnace (Shanghai Jujing, China, SGL-1700C) was used as the experimental equipment, and a corundum porcelain boat (120 mm in length, 60 mm in width, and 20 mm in height) was used as the material container in the present study. Chemical analysis of the experimental materials and roasting slags was performed using an ICP-OES (Optima 7300 V, Perkin Elmer, USA). The occurrence states of Zn and Pb in the copper smelting slag were determined by chemical phase analysis (China Changsha Institute of Mining and Metallurgy). The morphological characteristics of the roasting slags were determined using a scanning electron microscope (SEM) equipped with EDS. An XRD analyzer (D8 Discover 2500) using a PANalytical X'Pert X-ray diffractometer (Cu K_α radiation) was used. FactSage™7.1 software was used to establish the detailed thermodynamic modeling.

3 Results and discussion

3.1 Volatilization principle and thermodynamic analysis

To determine the feasibility of recovering Pb and Zn by chlorination roasting, the saturated vapor pressures of their chlorides, sulfides, and oxides must be calculated. The variation in the saturated vapor pressure as the temperature changes can be determined using the Antoine equation [28] (Eqs. (3)−(7)). The results are shown in Fig. 2 (the relevant calculation data for ZnO are unknown; however, it can be confirmed from the literature that ZnO is not volatile [29]). The saturated vapor pressure of chlorides was higher than that of sulfides and oxides. Therefore, Zn and Pb in the copper smelting slag could be separated and recovered during the chlorination roasting process.

$$\lg P_{PbCl_2} = 10000T^{-1} - 6.65\lg T + 33.52 \tag{3}$$

$$\lg P_{ZnCl_2} = 8415T^{-1} - 5.035\lg T + 28.545 \tag{4}$$

$$\lg P_{PbS} = -11597T^{-1} + 12.57 \tag{5}$$

$$\lg P_{PbO} = -13300T^{-1} - 0.81\lg T - 0.00043T + 16.93 \tag{6}$$

$$\lg P_{ZnS} = -13846T^{-1} + 12.7 \tag{7}$$

A thermodynamic reaction model of chlorination roasting was developed to understand the reaction process [30]. Combined with the preceding process mineralogy analysis of copper

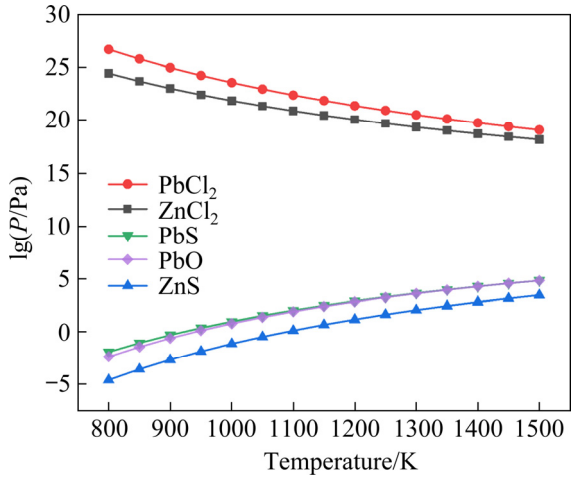

Fig. 2 Variation of saturated vapor pressure versus temperature

smelting slag, when using $CaCl_2$ as the chlorine donor, possible reactions in chlorination roasting process are shown in Eqs. (8)−(15). Details of thermodynamic modeling were undertaken using FactSage™7.1 software [31].

$$Zn_2SiO_4+2CaCl_2+SiO_2=2ZnCl_2(g)+2CaSiO_3 \quad (8)$$

$$ZnFe_2O_4+CaCl_2+SiO_2=ZnCl_2(g)+CaSiO_3+Fe_2O_3 \quad (9)$$

$$ZnS+CaCl_2=ZnCl_2(g)+CaS \quad (10)$$

$$ZnO+CaCl_2+SiO_2=ZnCl_2(g)+CaSiO_3 \quad (11)$$

$$PbSiO_3+CaCl_2=PbCl_2(g)+CaSiO_3 \quad (12)$$

$$PbS+CaCl_2=PbCl_2(g)+CaS \quad (13)$$

$$PbO+CaCl_2+SiO_2=PbCl_2(g)+CaSiO_3 \quad (14)$$

$$PbSO_4+CaCl_2=PbCl_2(g)+CaSO_4 \quad (15)$$

The conventional thermodynamic model is based on the constant partial pressure of gaseous products [32]. However, according to Eqs. (16) and (17), the Gibbs free energy change of the reaction in Eqs. (8)−(15) can be changed by controlling the partial pressure of gaseous products [33]:

$$\Delta G^{\Theta}=-RT\ln K^{\Theta}=-RT\ln\frac{P_{ZnCl_2}}{P^0} \quad (16)$$

$$\Delta G^{\Theta}=-RT\ln K^{\Theta}=-RT\ln\frac{P_{PbCl_2}}{P^0} \quad (17)$$

During the chlorination roasting process in the experiment, the air was blown into the experimental furnace to make the gaseous products ($ZnCl_2$ and $PbCl_2$) leave the reaction zone with the flowing gas, thereby decreasing the partial pressure of the gaseous products in the system and facilitating the positive direction of the reaction in Eqs. (8)−(15). If the partial pressures of the gaseous products were 1, 1/2, 1/10, 1/100, 1/1000, and 1/10000 of the total pressure, the Gibbs free energy change of the chlorination roasting process was calculated and is shown in Figs. 3(a–h). At a roasting temperature of 850 °C, the Gibbs free energy changes (ΔG) of these reactions were all positive. Therefore, as the effect of the partial pressure of gaseous products was considered, Zn and Pb in the copper smelting slag could be completely recovered from the chlorination roasting process [34]. In all the experiments, air was pumped at a constant rate (100 mL/min) into the furnace.

3.2 Statistical analysis

3.2.1 Model selection

Mathematical polynomial models can be divided into first-order, two-factor interactions, quadratic, cubic, and so on [35]. To evaluate the reliability of experimental results and the credibility of mathematical model, the experimental results must be tested for significance [36]. The model statistics are listed in Table 5. The adjusted R^2 values of the quadratic model corresponding to Zn and Pb were 0.9818 and 0.9972, respectively, indicating that 98.18% and 99.72% of the response value changes of the recovery ratios for Zn and Pb were attributed to the three factors and the model fit well with the actual situation. The value of $R^2_{adj(Zn)}$=0.9583 was close to $R^2_{(Zn)}$=0.9818 in the quadratic model of the recovery ratio for Zn, whereas the value of $R^2_{adj(Pb)}$=0.9936 was close to $R^2_{(Pb)}$=0.9972 in the quadratic model of the recovery ratio for Pb, indicating the high significance of the models [37]. Therefore, recovery ratio models are recommended for use in the quadratic model.

Table 6 gives the experimental data design matrix and the responses proposed by the Box−Behnken design with three factors at three levels. The plots in Fig. 4 depict the correlation between the predicted values obtained from Eq. (1), and the actual values of the experimental observations. The actual and predicted values were evenly distributed on both sides of the linear regression, indicating a good agreement between the actual and predicted values for the Zn and Pb

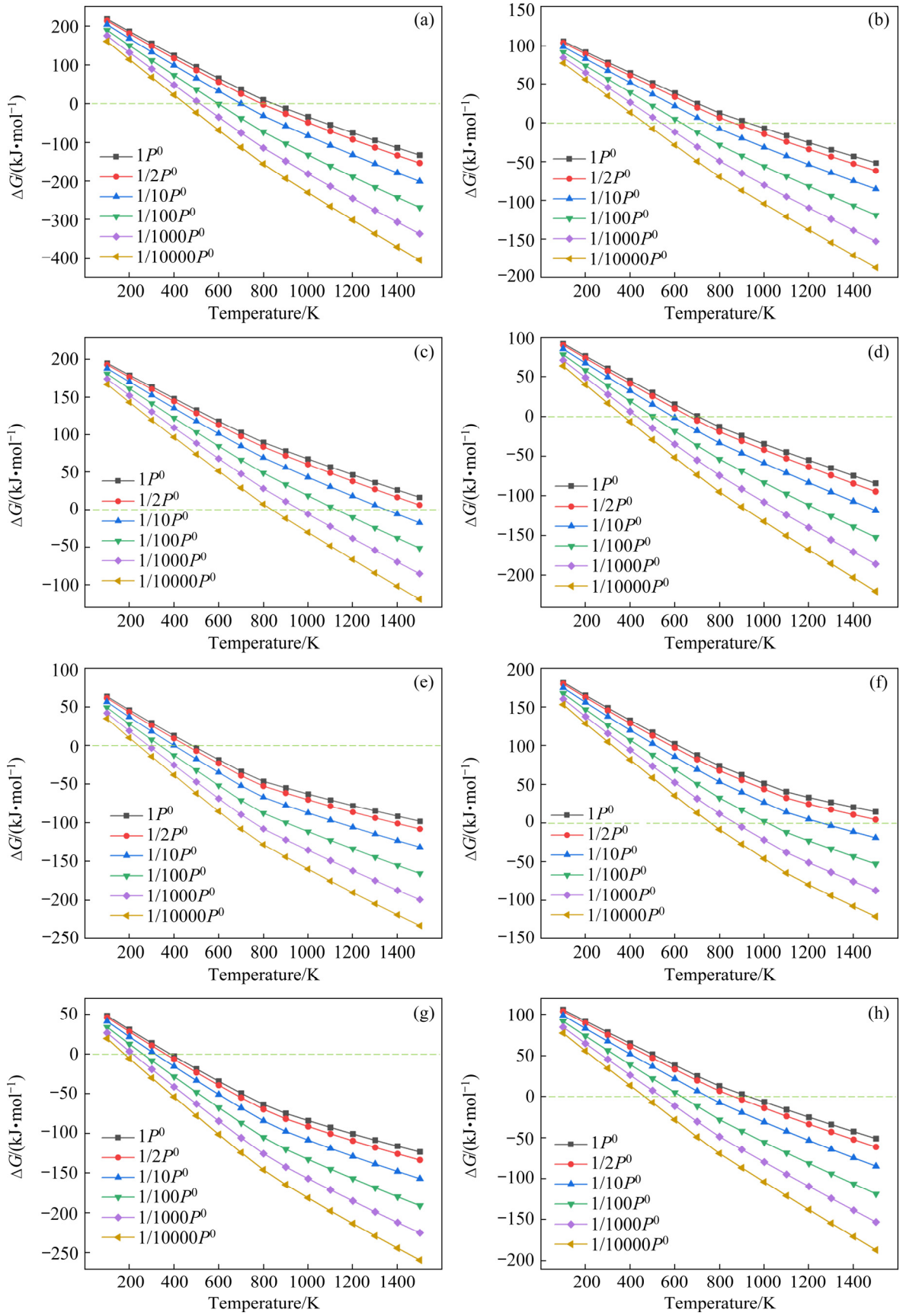

Fig. 3 Thermodynamic modeling of chlorination roasting at different partial pressures of gaseous products: (a) Zn_2SiO_4 (Eq. (8)); (b) $ZnFe_2O_4$ (Eq. (9)); (c) ZnS (Eq. (10)); (d) ZnO (Eq. (11)); (e) $PbSiO_3$ (Eq. (12)); (f) PbS (Eq. (13)); (g) PbO (Eq. (14)); (h) $PbSO_4$ (Eq. (15))

Table 5 Analysis of different response surface models

Metal	Source	Standard deviation	*R*-squared	Adjusted *R*-squared
Zn	Linear	11.82	0.8255	0.7852
	2FI	13.34	0.8288	0.7261
	Quadratic	5.20	0.9818	0.9583
Pb	Linear	14.47	0.6206	0.5331
	2FI	16.40	0.6252	0.4003
	Quadratic	1.69	0.9972	0.9936

Table 6 Box−Behnken experimental design matrix and results

No.	$w(CaCl_2)$/wt.%	Temperature/°C	Time/min	Zn recovery efficiency/%		Pb recovery efficiency/%	
				Observed	Predicted	Observed	Predicted
1	10	700	60	1.77	−4.26	42.50	42.29
2	30	700	60	29.04	27.24	53.46	51.85
3	10	1200	60	45.37	47.17	88.05	89.66
4	30	1200	60	80.18	86.21	96.85	97.06
5	10	950	30	38.35	38.76	91.25	89.49
6	30	950	30	73.65	69.82	99.41	99.05
7	10	950	90	31.46	35.29	93.80	94.16
8	30	950	90	75.18	74.77	99.81	101.57
9	20	700	30	15.41	21.04	44.43	46.40
10	20	1200	30	80.12	77.92	98.04	98.19
11	20	700	90	21.25	23.45	55.66	55.51
12	20	1200	90	82.61	76.98	98.24	96.27
13	20	950	60	67.76	65.38	98.33	97.90
14	20	950	60	64.59	65.38	97.59	97.90
15	20	950	60	64.36	65.38	97.59	97.90
16	20	950	60	64.97	65.38	97.79	97.90
17	20	950	60	65.20	65.38	98.19	97.90

recovery efficiencies. Thus, the quadratic model could accurately predict the test results [38].

3.2.2 Analysis of variance (ANOVA)

The ANOVA results for the regression model are given in Table 7. When the *P* value was lower than 0.05, the model and chosen variable were remarkable [39]. As seen in Table 7, the *P* values of the recovery efficiency models were lower than 0.0001, indicating that the credibility of the model was high. In the quadratic model of Zn, x_1, x_2, x_1^2, and x_2^2 were significant model items because their *P* values were lower than 0.05, whereas other linear, quadratic, and interactive terms were insignificant. Similarly, x_1, x_2, x_3, x_2x_3, x_1^2, and x_2^2 were significant model items in the quadratic model of Pb. The higher the *F* values are, the more significant the influence of the variables is [36]; therefore, the notable degrees for influencing the Zn recovery efficiency were the $CaCl_2$ dosage and roasting temperature. All independent variables were notable for influencing the Pb recovery efficiency. In addition, the coefficients of variation for Zn and Pb were 9.81% and 1.98%, respectively. The adequate precisions for Zn and Pb were 22.6717 and 45.794, respectively, confirming that the models can be used to predict Zn and Pb recovery efficiencies.

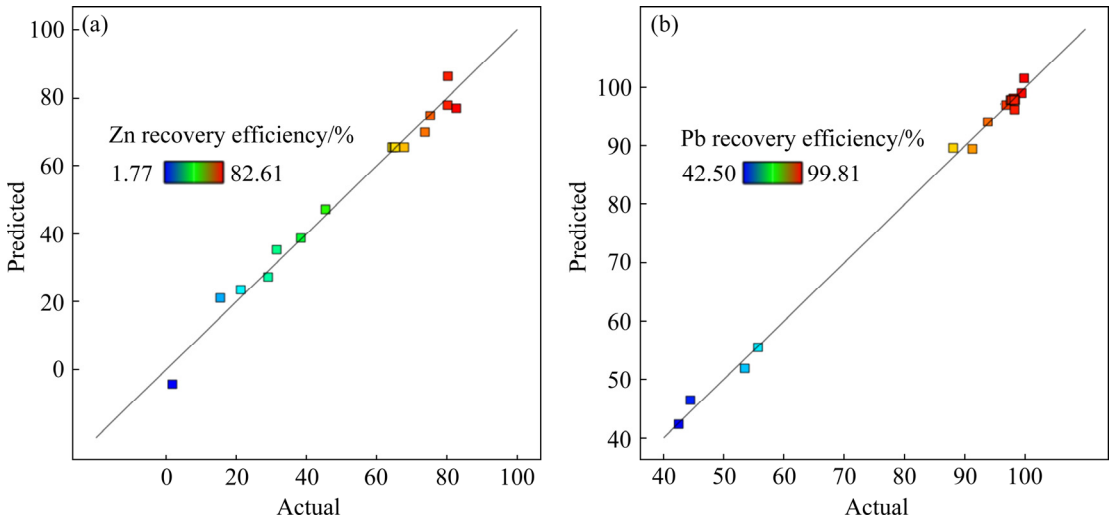

Fig. 4 Relationship between predicted values and actual values defined for experimental region of Zn recovery efficiency (a) and Pb recovery efficiency (b)

Table 7 Analysis of variance for response surface quadratic model

Metal	Source	Analysis					
		Sum of squares	Degree of freedom	Mean square	*F* value	*P* value	Conclusion
Zn	Model	10209.68	9	1134.41	41.90	<0.0001	Significant
	x_1	2488.65	1	2488.65	91.92	<0.0001	Significant
	x_2	6094.63	1	6094.63	225.10	<0.0001	Significant
	x_1^2	484.38	1	484.38	17.93	0.0039	Significant
	x_2^2	1018.02	1	1018.02	37.60	0.0005	Significant
	Residual	189.52	7	27.07			
	C.V.: 9.81%			Adequate precision: 22.6717			
Pb	Model	7156.55	9	795.17	279.17	<0.0001	Significant
	x_1	143.91	1	143.91	50.52	0.0002	Significant
	x_2	4284.14	1	4284.14	1504.08	<0.0001	Significant
	x_3	25.85	1	25.85	9.07	0.0196	Significant
	x_2x_3	30.42	1	30.42	10.68	0.0137	Significant
	x_1^2	34.30	1	34.30	12.04	0.0104	Significant
	x_2^2	2595.70	1	2595.70	911.30	<0.0001	Significant
	Residual	19.94	7	2.85			
	C.V.: 1.98%			Adequate precision: 45.7940			

3.2.3 Effect of roasting parameters and interactions

Based on the significant regression terms and their corresponding estimated coefficients, the regression equations for the metal recovery efficiency for each coded factor are given in Eqs. (18) and (19), describing the functional relationship between the response values and impact factors:

$$Y_{Zn}=65.38+17.64x_1+27.6x_2+0.3712x_3+1.88x_1x_2+2.11x_1x_3-0.8375x_2x_3-10.74x_1^2-15.55x_2^2+0.0208x_3^2 \quad (18)$$

$$Y_{Pb}=97.9+4.24x_1+23.14x_2+1.8x_3-0.54x_1x_2-0.5375x_1x_3-2.76x_2x_3-2.85x_1^2-24.83x_2^2+1.02x_3^2 \quad (19)$$

Based on the quadratic response functions, 3D surface plots and contour plots were used to illustrate the interaction of factors on response [40]. Figures 5(a–c) and 5(d–f) show the response surfaces for Zn and Pb recovery, respectively. As shown in Figs. 5(a, d), the $CaCl_2$ dosage and roasting temperature positively affected Zn and Pb recovery efficiencies with a roasting time of 60 min. Increasing the $CaCl_2$ dosage resulted in a gradual increase in metal recovery, especially for Zn. Similarly, the roasting temperature is an important parameter for improving metal recovery efficiency. However, when the temperature exceeded 1041 °C, increasing the roasting temperature reduced the Pb recovery efficiency. The roasting slags obtained at 700, 950, 1000, and 1050 °C were further analyzed using SEM, as shown in Fig. 6. At 700−1000 °C, the mineral surface gradually dissociated with increasing temperature, owing to the destruction of the frame of the copper smelting slag at high temperatures. At 700−1000 °C, the metal recovery efficiency increased with increasing temperature, attributed to the further exposed metals enhancing the mass transfer process of the chlorination reaction [18]. When the roasting temperature was increased to 1050 °C, the slag became dense, caused by sintering at high temperatures; therefore, the porosity of the mineral was reduced, hindering the chlorination reaction [41]. Thermodynamically, the chlorination reaction could be enhanced by increasing the temperature. From the response surface methodology results, at 700−1200 °C, the Zn recovery efficiency increased with increasing temperature, even if the mineral was sintered. Owing to the high Zn content in minerals, the adverse effect of sintering was lower than the favorable influence of thermodynamics. Conversely, at 1041−1200 °C, the Pb recovery efficiency decreased with increasing temperature because the sintering of the mineral hindered the chlorination reaction.

As shown in Figs. 5(b, e), an increase in the

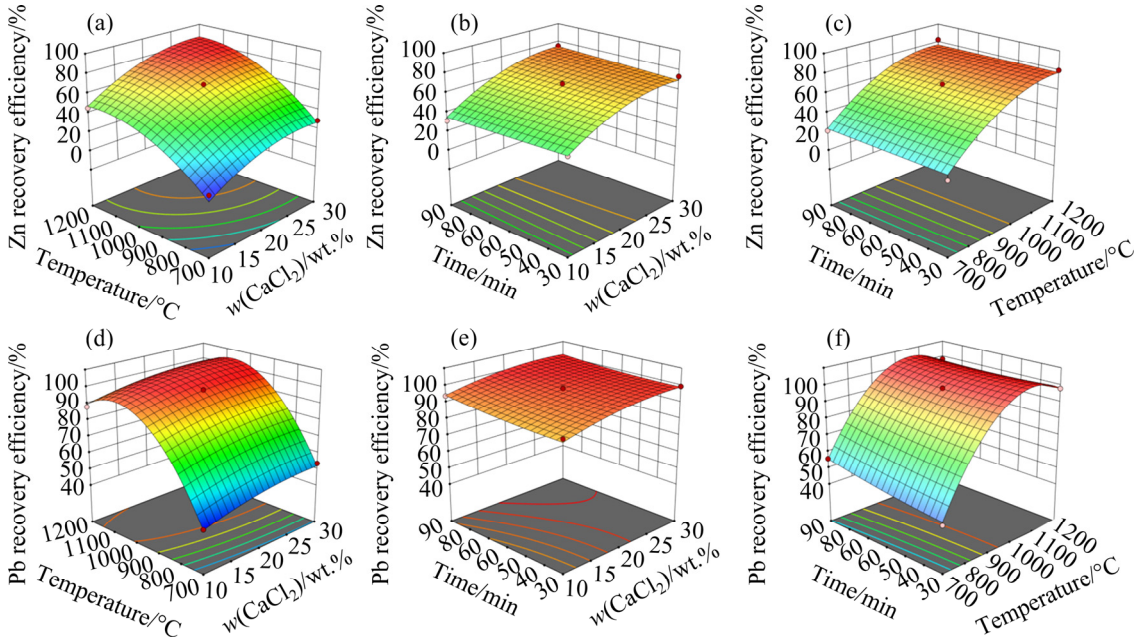

Fig. 5 Surface 3D plots for Zn recovery efficiency (a−c) and Pb recovery efficiency (d−f): (a, d) Time: 60 min; (b, e) Temperature: 950 °C; (c, f) 20 wt.% $CaCl_2$

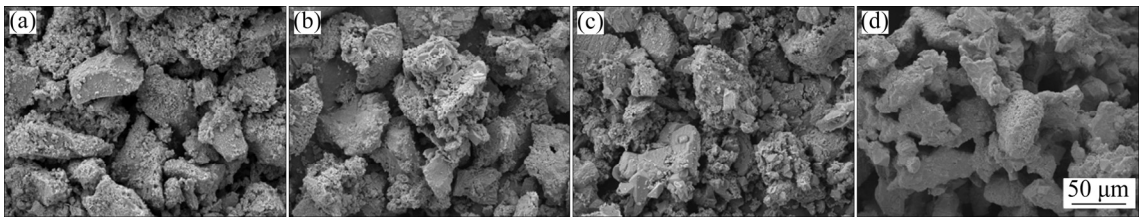

Fig. 6 SEM images of roasting slag roasted at different temperatures: (a) 700 °C; (b) 950 °C; (c) 1000 °C; (d) 1050 °C

roasting time increased Zn and Pb recovery efficiencies; therefore, extending the roasting time promoted the extent of the chlorination reaction and increased the metal recovery efficiency. Figures 5(c, f) confirmed that the temperature effect on the recovery rates of Zn and Pb was slightly different. In the range of 700−1200 °C, the Zn recovery efficiency increased as the temperature increased. For the Pb recovery efficiency, when the temperature was higher than 1079 °C, the Pb recovery gradually decreased as the temperature increased, and the reason was the same as above.

Meanwhile, Figs. 7(a–c) and 7(d–f) show the contour plots for Zn and Pb recovery, respectively. The contour shapes of the roasting temperature and $CaCl_2$ dosage were close to ellipses in Figs. 6(a, d), demonstrating that their interaction was significant. The contour shapes of the other factors were similar to straight lines, implying that their interaction was small [42].

3.2.4 Optimization

The optimum roasting conditions and the predicted recovery efficiencies were determined using Design-Expert12, as given in Table 8. Three experiments were conducted under optimal conditions to verify the optimized results. The average Zn and Pb recovery efficiencies obtained under optimized conditions were 87.85% and 99.26%, respectively. The results showed that the predicted values were in good agreement with the observed data, indicating that the model was statistically significant.

Due to the small amount of Zn and Pb components in the roasting slag, Zn- and Pb-containing phases could not be accurately detected by XRD. Therefore, SEM−EDS was utilized to analyze the micromorphology of the roasting slags when roasted at 1172 °C for 100 min, and $CaCl_2$ dosage was 30 wt.%. The results are shown in Fig. 8(a) and Table 9. The mineral existed in three typical areas (gray, white, and black), and white areas were enclosed in dark parts. The EDS-point results showed that Fe, Si, and O mainly occurred in the dark parts, whereas Zn mainly occurred in

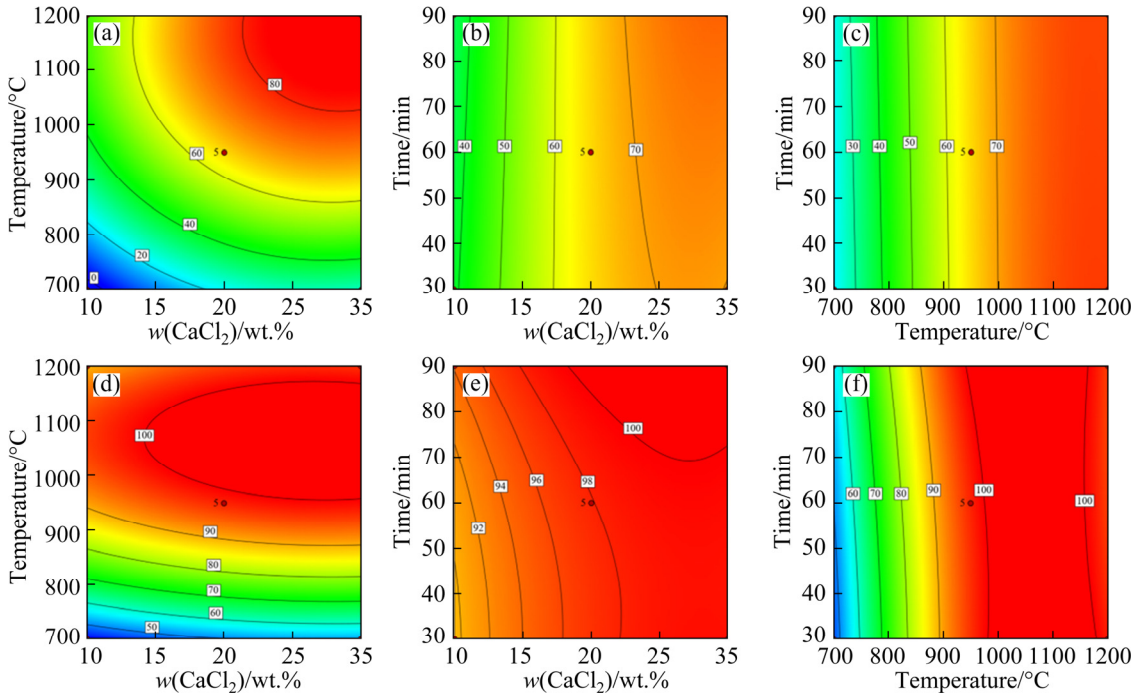

Fig. 7 Contour 2D plots for Zn recovery efficiency (a−c) and Pb recovery efficiency (d−f): (a, d) Time: 60 min; (b, e) Temperature, 950 °C; (c, f) 20 wt.% $CaCl_2$

Table 8 Optimum roasting conditions and results

$w(CaCl_2)$/wt.%	Temperature/°C	Time/min	Zn recovery efficiency/%		Pb recovery efficiency/%	
			Observed	Predicted	Observed	Predicted
30	1172	100	87.85	88.57	99.26	99.99

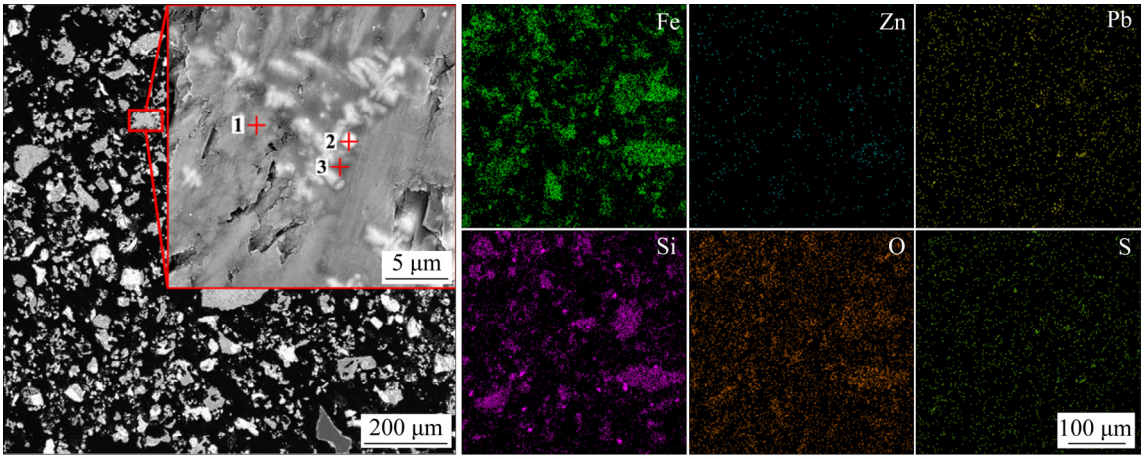

(a) (b)

Fig. 8 SEM−EDS images of roasting slag under optimum roasting conditions (a) and EDS mapping of roasting slag under optimum roasting conditions (b)

Table 9 Analytical results of roasting slag under optimum roasting conditions (wt.%)

Point in Fig. 8(a)	Fe	Si	O	Zn	Pb	Ca	S
1	39.61	21.09	26.55	5.31	1.91	1.06	0.34
2	17.87	16.31	15.59	26.08	2.04	2.98	10.64
3	18.62	26.25	30.62	2.35	2.11	12.96	1.15

the white areas. Therefore, the residual Zn-containing phase was a ternary (Fe−Zn−O) or quaternary compound (Fe−Zn−Si−O), and residual Pb-containing phase could not be accurately determined, because of the Pb traces in the slag.

EDS mapping of the roasting slags under the optimum roasting conditions is shown in Fig. 8(b). The elemental distributions of Fe, Si, and O were dispersive and homogeneous. The residual Zn was almost encapsulated in these elements, and the elemental distributions of Pb and S were analogous. In conclusion, the residual Zn- and Pb-containing phases might be $ZnFe_2O_4$, Zn_2SiO_4, and PbS. The raw material compounds could not be thoroughly chlorinated, which was consistent with thermodynamic calculation results.

4 Conclusions

(1) The thermodynamic reaction model of chlorination roasting indicated that Zn- and Pb-containing phases in copper smelting slag could be efficiently separated and recovered by decreasing the partial pressure of the gaseous products in the system.

(2) The Box-Behnken design was applied to assessing the interactive effects of the process variables and optimizing the chlorination roasting process. The ANOVA results demonstrated that the regression equations were appropriate for optimizing the independent variables within the range. The 3D surface plot and contour plot results indicated a notable influence of $CaCl_2$ dosage and roasting temperature on Zn and Pb recovery.

(3) The optimal chlorination roasting conditions for recovering Zn and Pb were 30 wt.% of $CaCl_2$ at 1172°C for 100 min. Under these conditions, the predicted Zn and Pb recovery efficiencies reached 87.85% and 99.26%, respectively, which matched well with the actual observed values. After the optimal chlorination roasting process, the residual Zn- and Pb-containing phases were inferred to be $ZnFe_2O_4$, Zn_2SiO_4, and PbS.

Acknowledgments

The authors are grateful for the financial supports from the National Natural Science Foundation of China (Nos. 51620105013, 51904351), Innovation-Driven Project of Central South University, China (No. 2020CX028), Natural

Science Fund for Distinguished Young Scholar of Hunan Province, China (No. 2019JJ20031), and the National Key R&D Program of China (No. 2019YFC1907400)

References

[1] PENG R Q. Metallurgy of lead and zinc [M]. Beijing: Science Press, 2003. (in Chinese)

[2] LI W F, ZHAN J, FAN Y F, WEI C, ZHANG C F, HWANG J Y. Research and industrial application of a process for direct reduction of molten high-lead smelting slag [J]. JOM, 2017, 69(4): 784−789.

[3] PAN D A, LI L L, TIAN X, WU Y F, CHENG N, YU H L. A review on lead slag generation, characteristics, and utilization [J]. Resources Conservation & Recycling, 2019, 146: 140−155.

[4] GUO X Y, TIAN Q H, LIU Y, YAN H J, LI D, WANG Q M, ZHANG J F. Progress in research and application of non-ferrous metal resources recycling [J]. The Chinese Journal of Nonferrous Metals, 2019, 29(9): 65−107. (in Chinese)

[5] ZHANG X U, YANG L S, LI Y H, LI H R, WANG W Y, GE Q S. Estimation of lead and zinc emissions from mineral exploitation based on characteristics of lead/zinc deposits in China [J]. Transactions of Nonferrous Metals Society of China, 2011, 21(11): 2513−2519.

[6] YANG S J, ZHANG L W, YU D H. Intensive development and comprehensive utilization of metallurgical slag [J]. Applied Mechanics & Materials, 2012, 174−177: 1424−1428.

[7] HU M, PENG B, CHAI L Y, LI Y C, PENG N, YUAN Y Z, CHEN D. High-zinc recovery from residues by sulfate roasting and water leaching [J]. JOM, 2015, 67(9): 2005−2012.

[8] XIN P F, WEI J Y, XU L, WU W G, LAN D L. The recovery of Pb and Zn in antimony smelting slag [M]. PbZn 2020: 9th International Symposium on Lead and Zinc Processing. San Diago, USA: Springer-TMS, 2020.

[9] PENG B, PENG N, LIU H, XUE K, LIN D H. Comprehensive recovery of Fe, Zn, Ag and In from high iron-bearing zinc calcine [J]. Journal of Central South University, 2017, 24: 1082−1089.

[10] ZHANG J L, YANG X, ZHANG J K, CHEN Y Q, ZHANG L F, WANG C Y. Influence of slag contents on sedimentation separation of slag and matte at high temperature [J]. The Chinese Journal of Nonferrous Metals, 2019, 29(8): 1712−1720. (in Chinese)

[11] WANG H Y, SONG S X. Separation of silicon and iron in copper slag by carbothermic reduction−alkaline leaching process [J]. Journal of Central South University, 2020, 27(8): 2249−2258.

[12] SUN W, SU J F, ZHANG G, HU Y H. Separation of sulfide lead−zinc−silver ore under low alkalinity condition [J]. Journal of Central South University, 2020, 27(8): 2249−2258.

[13] LI G S, ZOU X L, CHENG H W, GENG S H, XIONG X L, XU Q, ZHOU Z F, LU X G. A novel ammonium chloride roasting approach for the high-efficiency Co-sulfation of nickel, cobalt, and copper in polymetallic sulfide minerals [J]. Metallurgical and Materials Transactions B, 2020, 21: 2769−2784.

[14] DING J, HAN P W, LU C C, QIAN P, YE S F, CHEN Y F. Utilization of gold-bearing and iron-rich pyrite cinder via a chlorination−volatilization process [J]. International Journal of Minerals, Metallurgy, and Materials, 2017, 24(11): 1241−1250.

[15] MUKHERJEE T K, GUPTA C K. Base metal resource processing by chlorination [J]. Mineral Processing and Extractive Metallurgy Review, 1983, 1(1−2): 111−153.

[16] JENA P K, BROCCHI E A. Base metal extraction through chlorine metallurgy [J]. Mineral Processing and Extractive Metallurgy Review, 2008, 16(4): 211−237.

[17] WANG H J, FENG Y L, LI H R, KANG J X. Simultaneous extraction of gold and zinc from refractory carbonaceous gold ore by chlorination roasting process [J]. Transactions of Nonferrous Metals Society of China, 2020, 30(4): 1111−1123.

[18] QIN H, GUO X Y, TIAN Q H, ZHANG L. Pyrite enhanced chlorination roasting and its efficacy in gold and silver recovery from gold tailing [J]. Separation and Purification Technology, 2020, 250: 117168.

[19] LI H Y, PENG J H, LONG H L, LI S W, ZHANG L B. Cleaner process: Efficacy of chlorine in the recycling of gold from gold containing tailings [J]. Journal of Cleaner Production, 2021, 287: 125066.

[20] ZHU M L, XIAO N, TANG L C, ZHONG S P, LÜ X L, CHI X P. Preparation of new cementitious material by reduction and activation of copper slag and its application in mine filling [J]. The Chinese Journal of Nonferrous Metals, 2020, 30(11): 2736−2745. (in Chinese)

[21] WHITTINGHILL D C. A note on the robustness of Box−Behnken designs to the unavailability of data [J]. Metrika, 1998, 48(1): 49−52.

[22] HAO X D, LIU X D, YANG Q, LIU H W, YIN H Q, QIU G Z, LIANG Y L. Comparative study on bioleaching of two different types of low-grade copper tailings by mixed moderate thermophiles [J]. Transactions of Nonferrous Metals Society of China, 2018, 28(9): 1847−1853.

[23] DU K, WANG C Y, WANG L. Distribution of main elements and phase characteristics of copper converter slag [J]. Journal of Central South University (Science and Technology), 2018, 49(11): 2649−2655. (in Chinese)

[24] FATMA U, FARUK K. Modelling of relation between synthesis parameters and average crystallite size of Yb_2O_3 nanoparticles using Box−Behnken design [J]. Ceramics International, 2020, 46(17): 26800−26808.

[25] ZHOU H, XU J N, ZHOU M X, NI Y G. Study on immobilization of heavy metals in a waste SCR catalyst during high temperature melting treatment [J]. Journal of Chinese Society of Power Engineering, 2020, 40(6): 492−501.

[26] JAAFAR I, GRIFFITHS A J, HOPKINS A C, STEER J M, GRIFFITHS M H, SAPSFORD D J. An evaluation of chlorination for the removal of zinc from steelmaking dusts [J]. Minerals Engineering, 2011, 24(9): 1028−1030.

[27] MYERS R H, MONTGOMERY D C, ADWESON-COOK C

M. Response surface methodology: Process and product optimization using designed experiments [M]. New York: John Wiley and Sons, Inc, 2008.

[28] DONG Z W, XIONG H, DENG Y, YANG B, ZHAO J Y, DAI Y N, WANG J J. Separation and enrichment of PbS and Sb_2S_3 from jamesonite by vacuum distillation [J]. Vacuum, 2015, 121: 48−55.

[29] DAI Y N, YANG B, MA W H, CHEN W L, DAI J Q. Advances on vacuum metallurgy of nonferrous metals [J]. Engineering Sciences, 2004, 2(3): 12−19, 29.

[30] YANG X M, LI J Y, WEI M F, ZHANG J. Thermodynamic evaluation of reaction abilities of structural units in Fe−O binary melts based on the atom-molecule coexistence theory [J]. Metallurgical and Materials Transactions B, 2016, 47(1): 174−206.

[31] BALE C W, BÉLISLE E, CHARTRAND P, DECTEROV S A, ERIKSSON G, GHERIBI A E, HACK K, JUNG I H, KANG Y B, MELANÇON J, PELTON A D, PETERSEN S, ROBELIN C, SANGSTER J, SPENCER P, van ENDE M A. FactSage thermochemical software and databases, 2010—2016 [J]. Calphad, 2016, 54: 35−53.

[32] HUANG X H. Principles on ferrous metallurgy [M]. Beijing: Metallurgical Industry Press, 2013. (in Chinese)

[33] LI H G. Metallurgical principle [M]. Beijing: Science Press, 2005. (in Chinese)

[34] DONG Z W, XIA Y, GUO X Y, ZHAO J L, JIANG L F, TIAN Q H, LIU Y. Direct reduction of upgraded titania slag by magnesium for making low-oxygen containing titanium alloy hydride powder [J]. Powder Technology, 2020, 368: 160−169.

[35] MA Z Y, YANG H Y. Microwave assisted leaching of selenium from copper anode slime optimized by response surface methodology [J]. Journal of Central South University: Science and Technology, 2015, 46(7): 2391−2397. (in Chinese)

[36] HUO Q, LIU X, CHEN L J, WU Y H, WU H Y, XIE J P, LIU X X, QIU G Z. Treatment of backwater in bauxite flotation plant and optimization by using Box−Behnken design [J]. Transactions of Nonferrous Metals Society of China, 2019, 29(4): 821−830.

[37] NAIR A T, AHAMMED M M. Coagulant recovery from water treatment plant sludge and reuse in post-treatment of UASB reactor effluent treating municipal wastewater [J]. Environmental Science and Pollution Research, 2014, 21(17): 10407-10418.

[38] YANG S Y, LI Y, JIA D Y, YAO K, LIU W J. The synergy of Box-Behnken designs on the optimization of polysaccharide extraction from mulberry leaves [J]. Industrial Crops and Products, 2017, 99: 70−78.

[39] GHASEMI S, FARHADIZADEH A R, GHOMI H. Effect of frequency and pulse-on time of high power impulse magnetron sputtering on deposition rate and morphology of titanium nitride using response surface methodology [J]. Transactions of Nonferrous Metals Society of China, 2019, 29(12): 2577−2590.

[40] XU Z P, GUO X Y, LI D, TIAN Q H, ZHU L. Optimization of tellurium and antimony extraction from residue generated in alkaline sulfide leaching of tellurium-bearing alkaline skimming slag using central composite design [J]. Mining Metallurgy and Exploration, 2020, 37: 493−505.

[41] ZHOU Y N, YAN D H, LI L, CONG J, WANG N, PENG Z, WANG Q. Volatile characteristics of lead and zinc during co-processing hazardous waste in sintering machines [J]. Acta Scientiae Circumstantiae, 2015, 35(11): 3769−3774. (in Chinese)

[42] CIFUENTES B, FIGUEREDO M, COBO M. Response surface methodology and aspen plus integration for the simulation of the catalytic steam reforming of ethanol [J]. Catalysts, 2017, 7(1): 15−34.

从氯化焙烧铜熔炼渣中回收锌和铅的热力学分析及工艺优化

张倍恺[1]，郭学益[1,2,3]，王亲猛[1,2,3]，田庆华[1,2,3]

1. 中南大学 冶金与环境学院，长沙 410083；
2. 有色金属资源循环利用国家地方联合工程研究中心，长沙 410083；
3. 有色金属资源循环利用湖南省重点实验室，长沙 410083

摘 要：提出一种高效回收铜熔炼渣中 Zn、Pb 金属的氯化焙烧工艺。建立可揭示氯化焙烧过程中有效回收 Zn、Pb 的热力学模型。通过减小气相产物分压，可以促进氯化焙烧反应。选取 $CaCl_2$ 用量、焙烧温度和时间作为工艺变量，Zn 和 Pb 的回收率作为响应，采用 Box−Behnken 设计评估各工艺变量间的相互作用关系，优化氯化焙烧工业。最佳工艺条件为 $CaCl_2$ 用量 30%(质量分数)、焙烧温度 1172 °C 和焙烧时间 100 min，在此条件下，锌和铅的回收率分别为 87.85%和 99.26%，该结果与实验结果相吻合。焙烧渣中存在 $ZnFe_2O_4$、Zn_2SiO_4 和 PbS 含 Zn、Pb 相。

关键词：氯化焙烧；铜熔炼渣；热力学模型；优化；锌铅回收；Box−Behnken 设计

(Edited by Bing YANG)